Politecnico di Torino

Porto Institutional Repository

[Article] Transport and Retention of High Concentrated Nano-Fe/Cu Particles Through Highly Flow-Rated Packed Sand Column

(Article begins on next page)

Transport and Retention of High Concentrated Nano-Fe/Cu Particles Through Highly Flow-Rated Packed Sand Column

Seiyed Mossa Hosseini[†,1], Tiziana Tosco[††]

[†] Assistant Professor, Natural Geography Department, University of Tehran, Tehran, P.O.Box: 14155-6465, Iran.

[††] Assistant Professor, Dipartimento di Ingegneria dell'Ambiente, del Territorio e delle Infrastrutture, Politecnico di Torino,Torino, Italy.

---

[1] Corresponding Author: Seiyed Mossa Hosseini (Email: *smhosseini@ut.ac.ir*)

Abstract

The design of an efficient field-scale remediation based on the use of nanoscale zero valent iron (NZVI) requires an accurate assessment of the mobility of such particles in saturated porous media, both during injection in the subsurface (short-term mobility) and later (long-term mobility). In this study, the mobility of highly concentrated dispersions of bimetallic *Fe/Cu* nanoparticles ($d_{50}= 70\pm5$ *nm*) in sand-packed columns (0.5 *m* length and 0.025 *m* inner diameter) was studied. In particular, the influence of flow rate ($V = 5\times10^{-4}$, 1×10^{-3}, 2×10^{-3} *m/s*) and injected particle concentrations (2, 5, 8, 12 *g/l*) was addressed. Breakthrough curves and water pressure drop along the column, averaged effective porosity and final distribution of retained particles along the column were measured. Experimental results evidenced a good mobility of the *Fe/Cu* particles, with significant breakthrough in all explored experimental conditions of flow rate and C_0, without requiring the addition of any stabilizing agent. Clogging phenomenon of the column and also the pore pressure variation during injection period are strongly affected by injected concentration. Clogging due to deposition of particles following a ripening dynamics was observed in particular for $C_0= 8$ and 12 *g/l*. The experimental data were modeled using the E-MNM1D software. The study has implications for field injection of bimetallic nanoparticles, suggesting that particular care is to be devoted when selecting injection concentration, to avoid porous medium clogging and control the radius of influence.

Abbreviations: Nanoscale zero valent iron, NZVI; Copper, Cu; Iron, Fe; Enhanced Micro- and Nanoparticle transport Model, E-MNM1D; Nitrate, NO_3^-; Polyvinyl Alcohol-Co-Vinyl Acetate-Co-Itaconic Acid, PV3A; Deep bed filtration theory; Sea water intrusion: SEAWAT; Emmett and Teller Method, BET; Hydrochloric acid, HCl; Pore volumes, PV; Specific surface area, SSA; Ultra violet visible, UV-Vis, Averaged effective porosity, AEP.

Graphical abstract
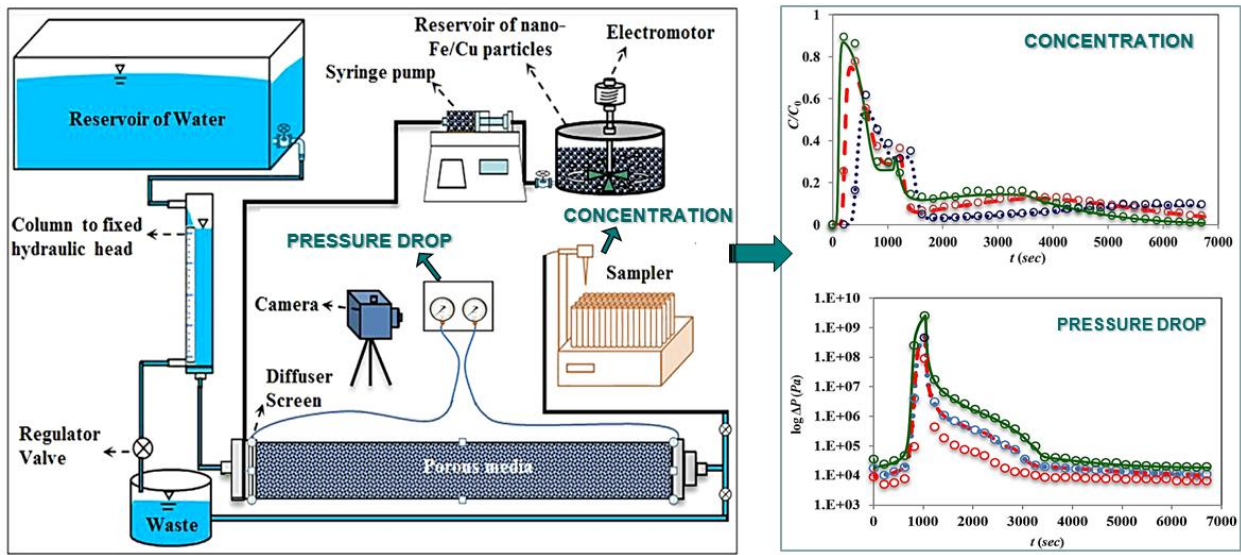
Highlights:

* Nano-Fe/Cu particles easily transport in the sand medium without significant retention.
* Clogging phenomenon follows a ripening dynamics is affected by injected concentration.
* Flow rate had a minor impact on the clogging phenomenon of the porous medium.
* EMNM1D code is able to simulate the transport mechanism of Fe/Cu particles.
* Injection concentration of the particles controls the radius of influence.

1. Introduction

Nanoscale zero valent iron (NZVI)-based technologies are studied for the in-situ remediation of contaminated aquifers: thanks to the small size, these particles can be effectively injected into the subsurface for the direct treatment of contaminated zones and sources (Zhang, 2003, Saleh *et al.*, 2007, Hee and Cha, 2008). Moreover, the extremely high specific surface area (SSA) provides a much higher surface reactivity compared to the more widely used millimetric iron (Zhang, 2003; Liu *et al.*, 2005; Freyria *et al.*, 2011). However, NZVI faced critical problems for applications in porous media: short travel distances, pore plugging and significant loss of porosity and permeability, especially when used in high concentrations, were observed at both laboratory and field scale (Cantrell *et al.* 1997, Zhang *et al.*, 2009, Noubactep *et al.*, 2011). This was attributed to the strong tendency of NZVI bare particles to aggregation, agglomeration, and consequent rapid settlement or filtration on the solid phase surface (Phenrat *et al.*, 2007; Tiraferri and Sethi, 2008). Researches show that bare iron nanoparticles may travel in porous media only a few centimeters far from the injection point under typical groundwater conditions (Tratnyek and Johnson, 2006; Tiraferri *et al.*, 2008; Dalla Vecchia *et al.*, 2009a). To overcome this critical issue, many efforts have been carried out to prepare a stable suspension of NZVI by using polymeric surface modifiers or anionic surface chargers, (Kanel *et al.*, 2007; Sun *et al.*, 2007; He and Zhao, 2005; Dalla Vecchia *et al.*, 2009b; Saleh *et al.*, 2008; Tiraferri *et al.*, 2008; Tiraferri and Sethi, 2009), or directly modifying the particle surface during synthesis by addition of noble metals (Elliott and Zhang, 2001, Yang and Lee, 2005; Hosseini *et al.*, 2011; Hosseini *et al.*, 2012). In the latter approach, the presence of composition heterogeneities on the particles surface provided in many cases better performances in terms of colloidal stability. Moreover, bimetallic NZVI showed much higher degradation rates towards all contaminants traditionally treated by

millimetric iron, including chlorinated organic compounds, halogenated hydrocarbons, heavy metals, radionuclides, and inorganic anions (Gillham and O'Hannesin, 1994; Zanetti and Fiore, 2005), and in many cases even better performances if compared to unmodified NZVI particles (Zhang, 2003; Wan and Chen, 1999, Tratnyek *et al*., 2003, Liou *et al*. 2005, Noubactep *et al*., 2011).

A number of column experiments is reported in the literature aimed to investigate the mobility of polymer-modified NZVI in one and two dimensional water-saturated porous media, under different hydrochemical and flow conditions (Sun *et al*., 2001; Tufenkji and Elimelech, 2004 b; Dalla Vecchia *et al*., 2009b; Phenrat *et al*., 2010; Caldelas, 2010; Tosco *et al*., 2012). The transport and deposition behavior of surface-modified NZVI in porous media is typically studied at low particle concentration (<30 *mg/l*) and often modeled using approaches based on clean bed filtration theory (CFT) (Saleh *et al*., 2008, Wang *et al*., 2008, Tufenkji and Elimelech, 2004a). In the CFT model, the removal of suspended particles is described by first-order kinetics, resulting in concentrations of suspended and retained particles that decay exponentially with distance (Tufenkji and Elimelech, 2004 b; Kim *et al*., 2007; Tian *et al*., 2010). However, under many circumstances, and in particular for highly concentrated colloidal suspensions of NZVI (i.e. for typical concentrations used in NZVI applications, in the order of *g/l*), deposition does not follow linear, irreversible kinetics like those considered in the CFT model, and blocking and ripening deposition dynamics are often observed (Li *et al*., 2008,). Also, in the presence of particle-particle attractive interactions, filtration and/or straining of agglomerates may become the most relevant mechanism controlling NZVI transport (Phenrat *et al*., 2009, Jaisi *et al*., 2008). The consequence is a progressive porosity and permeability decrease, until the complete clogging of the porous medium (Kanel *et al*., 2008, Noubactep *et al*., 2011, Tosco and Sethi, 2010).

Therefore, the assumptions of CFT are not likely to be valid for surface modified NZVI transport at high particle concentration (Phenrat *et al*., 2009), and other modeling approaches are to be considered. Kanel *et al*. (2007) used the variable-density code SEAWAT for simulating the transport of polymer (PAA) modified NZVI through homogenous porous media in 2-D scale. Tosco and Sethi (2010) developed the E-MNM1D software, which solves one dimensional transport with modified advection-dispersion-deposition equations to simulate the highly concentrated NZVI dispersed in a non-Newtonian gel of xanthan gum through saturated porous media.

In this work, bimetallic nanoparticles are used, constituted by a core of Fe^0 partly coated by Cu, named as nano-*Fe/Cu* particles. The presence of a partial coating of Cu was found to be responsible for longer reactivity lifetime, along with prevention or reduction of the formation and accumulation of toxic byproducts (Yang and Lee, 2005; Hosseini *et al*., 2011; Tratnyek *et al*., 2003). The mechanism responsible for this reactivity is related to catalytic hydrogenation and electrochemical effect (Wan and Chen, 1999; Ruangchainikom *et al*., 2006). Moreover, unlike most part of the nanoscale Fe^0 particles used in laboratory studies and field applications, the nano-*Fe/Cu* particles used in this study exhibited a good colloidal stability against sedimentation and aggregation, even at high concentrations, and consequently do not require the use of any stabilizing agent.

The objective of this study is to investigate the mobility and deposition behavior of highly concentrated suspensions of the nano-*Fe/Cu* particles, which previously showed good performances in terms of reactivity towards contaminants. In particular, the influence of injected concentration and pore velocity on the particle mobility was studied. Transport tests in sand-packed saturated columns were performed by injecting the bimetallic NZVI dispersed in natural

6

groundwater at different concentrations ($C0$ = 2, 5, 8, and 12 g/l) and different pore water velocity values (V= 5×10-4, 1×10-3, and 2×10-3 m/s). The E-MNM1D software was then used for inverse simulation of the experimental results. This research contributes to a better understanding of fundamental processes and important parameters governing nano-*Fe/Cu* particles transport and retention in coarse sand and provides experimental data for the development of nanoparticle transport models.

2. Materials and Methods

2.1. Nano-*Fe/Cu* particles

Surface-modified nano-*Fe/Cu* particles for column transport tests were synthesized following the protocol described in Hosseini *et al*. (2011). The particles have an NZVI core with a discontinuous *Cu* shell. The percentage of the *Cu* content can be tuned during synthesis. In this work, a percentage of 5% (*w/w*) was adopted, which previous studies demonstrated to provide higher contaminant reduction rates compared to other values (Liu *et al*., 2005; Hosseini *et al*., 2011). The characterization of the synthesized nano-*Fe/Cu* particles indicated an average diameter d_{50} = 70 ± 5 nm, a BET surface area SA= 28.6 m^2/g (or 2.14 × 10^8 m^2/m^3), and a particle density ρ_p = 7550 kg/m^3 (see Table 1).

2.2. Experimental apparatus and test procedure

A plexi-glass column (inner diameter D = 0.025 m) was repeatedly wet–packed to a total column length L = 0.5 m with a homogenous natural coarse sand (d_{50}= 0.83×10-3 m) with negligible iron content. Sand was packed in 10 layers, each layer with height of 0.05 m using vibration to minimize any layering or air entrapment and then flushed with a 1mM HCl solution at 10 pore

volumes (PV) in order to obtain a uniform surface charge in sand. Transport tests performed injecting a conservative tracer indicated a porosity (n) equal to 0.37 and a longitudinal dispersivity (α_L) equal to 5.7×10^{-3} m (see tracer tests in the Appendix section). Other relevant porous medium properties included bulk density (ρ_b) of 1682 kg/m^3, hydraulic conductivity (K) of 5.5×10^{-4} m/s (47.5 m/d) and permeability (k) of 5.6×10^{-11} m^2 (see Table A1 in the Appendix section).

The transport tests of the nano-*Fe/Cu* particles included three steps, namely pre-conditioning of the column with particle-free solution (~10-12 PVs), NZVI injection (1050 s), and flushing with the same particle-free solution (5700 s). In pre-conditioning and flushing steps, the natural groundwater of Karaj city (Iran) with ionic strength (I) of 40 mM was used. Each column test was performed at three constant flow rates, namely $V = 5 \times 10^{-4}$, 1×10^{-3}, and 2×10^{-3} m/s (corresponding to 43.2, 86.4, and 172.8 m/day, respectively). Table (A1) in the Appendix section summarizes the parameters values for porous medium, water, nanoparticles and also operation conditions of the experiments presented in this study.

The *Fe/Cu* nanoparticles concentration and the flow rate were chosen coherently with the purpose of initial study to design a remediation system in an aquifer system close to the city of Karaj (Iran) in the future. Un-uniformed groundwater direction in this aquifer caused that the remediation during the nanoparticles transport is more favorite than other in-situ remediation methods (e.g., reactive wall, permeable reactive barrier). The aquifer, which provides the tap water supply for ~2 million peoples, is heavily impacted by nitrates as a major contaminant. As a consequence, *Fe/Cu* nanoparticles were considered for the remediation of this aquifer. Basing on the maximum background NO_3^- concentration in the Karaj city aquifer (200 mg/l), values of $C_0 = 2$, 5, 8 and 12 g l^{-1} of nano-*Fe/Cu* particles were selected in this study, which lead to

stoichiometric ratio of *Fe/N*, respectively equal to 10, 25, 40 and 60. In addition, the pore water velocities of 5×10^{-4}, 1×10^{-3}, and 2×10^{-3} *m/s* were chosen as representative of the water velocity at a few meters from pumping wells $((2.5\text{-}6)\times10^{-3}$ *m/s*) and also at pumping well face screens (1.5-4.0×10^{-2} *m/s*) according to Freeze and Cherry (1979) and Bear (1979).

A constant water discharge through the sand-packed column was ensured by tuning the water level in two piezometers at the inlet and outlet of the column itself. Two valves after the water column was used for more convenience of the pressure gradient controlling during the experiment (see Figure A1). NZVI particles were injected in the column using a typical syringe pump at different flow rates. A permeable glass diffuser screen was used at the column inlet to provide a uniform distribution in the cross section. The NZVI suspensions were prepared by dispersing the nanoparticles in de-ionized and de-oxided water immediately prior the injection, and stored in a reservoir which was slowly, continuously stirred to prevent any sedimentation of the particles. The combination of three different flow rates ($V = 5\times10^{-4}$, 1×10^{-3}, and 2×10^{-3} *m/s*) and four different NZVI concentrations ($C_0 = 2, 5, 8,$ and 12 *g/l*) resulted in a total number of 12 transport tests.

The effluent concentration of NZVI particles was monitored by collecting 5 *ml* samples at specified time intervals using an automated sampling collector, and then total iron particles in solution was analyzed using an *UV-Vis* spectrophotometer (Shanghai Selon Sceince Instrument Co. Ltd., Model No. S22PC) with λ=508 *nm* after acid digestion using an adaptation of the approach taken in several recent studies on the stability of nZVI in solution as described in Saleh *et al*. (2008) and Johnson *et al*. (2009). The pressure drop along the column during the experiment was continuously measured by two pressure gauges connected at the column inlet and outlet

through plastic tubes, and monitored by a camera (as shown in the graphical abstract). To prevent the particles from entering, a synthetic fine pore sponge was applied at the pipes' inlet. The column tests were run in duplicates. For all tests, the breakthrough curves (BTC) of C/C_0 and pressure drop of water flowing through the sand column (ΔP) were measured over time. The spatial distribution of the retained NZVI concentration along the column (S vs x) was obtained only for the experiments with $C_0 = 8$ g/l, for the three considered flow rates $V = 5 \times 10^{-4}$, 1×10^{-3}, and 2×10^{-3} m/s at the end of injection period ($t=t_{inj}$) for one replicate, and at the end of the experimental time ($t_{exp}=t_{inj}+t_{flush}$) for the other replicate. At each case, the sand column was dissected into 10 sections of 0.05 m each minimizing the disturbance to the packed bed. The total concentration of deposed iron in each part was determined using the phenanthrolin colorimetric according to method of Johnson *et al.* (2009).

2.3. Mathematical model for one dimensional flow and colloid transport

The one-dimensional transport of suspended particles through porous media is usually modeled with a modified form of the advection-dispersion partial differential equation, including the interactions with the soil matrix (Bradford et al., 2003, Johnson and Elimelech, 1995, Tosco *et al*., 2009, Tiraferri *et al*., 2011), resulting from deposition (attachment) and release (detachment) of particles onto and from the solid matrix. In this work the following set of equations was adopted, considering two reversible interaction mechanisms:

$$
\begin{cases}
\dfrac{\partial}{\partial t}(\varepsilon C) + \dfrac{\partial}{\partial t}(\rho_b s) = \dfrac{\partial}{\partial x}(qC) + \dfrac{\partial}{\partial x}\left(\varepsilon D_x \dfrac{\partial C}{\partial x}\right) \\[4mm]
\dfrac{\partial}{\partial t}(\rho_b s_1) = \varepsilon k_{a1}\left(1 + A_1 s_1^{\beta_1}\right)C - \rho_b k_{d1}s_1 \\[4mm]
\dfrac{\partial}{\partial t}(\rho_b s_2) = \varepsilon k_{a2}\left(1 + \dfrac{x}{d_{50}}\right)^{\beta_2} C - \rho_b k_{d2}s_2
\end{cases}
\tag{1}
$$

where x [L] and t [T] are the independent variable for space and time, respectively. The dependent variables are the concentration of particles suspended in the fluid phase C [$M\,L^{-3}$] and the concentration of particles deposited on the soil matrix s, reported as mass of particles per unit mass of porous medium [-]. The porous medium parameters include the hydrodynamic dispersion D_x [$L^2\,T^{-1}$], the Darcian flow velocity q [$L\,T^{-1}$], the porous medium bulk density ρ_b [ML^{-3}], the effective porosity ε [-], and the mean diameter of the porous material d_{50} [L]. The kinetic model coefficients include the deposition and release rate coefficients for the ith interaction site k_a^i and k_d^i [T^{-1}] ($i = 1, 2$) and the multiplier and exponent coefficients defining the interaction dynamics, A_i and β_i [-].

The first equation represents the mass balance for the liquid phase, and the second and third equations the mass balances for the solid phase for the two interaction sites ($s = s_1 + s_2$). Site 1 (s_1) is modeled following the general formulation for physical-chemical interactions proposed by Tosco and Sethi (2010), which can be adapted to all commonly used interaction kinetics (first-order deposition dynamics, blocking, ripening). Site 2 (s_2) considers space-dependent deposition dynamics, modeled on the straining kinetics proposed by Bradford *et al.* (2003).

As previously discussed by several authors (Saleh *et al.*, 2007; Kanel *et al.* 2008; Tosco and Sethi, 2010), the transport of highly concentrated suspensions of iron nanoparticles through porous media often results in the deposition of a relevant fraction of the suspended particles.

High concentrations of retained particles can be due to a number of concurrent phenomena, including formation of aggregates in the pore space, which then are filtered and/or strained by the porous medium, or to attractive particle-particle interactions, which cause deposited particles to attract the suspended one, thus resulting in ripening phenomena. As a consequence, the presence of particle deposits may negatively affect the hydrodynamic parameters of the porous medium, resulting in clogging phenomena.

Clogging phenomena have a macroscopic effect on pressure gradient, defined by the Darcy's law. An overview of experimental data (Mays and Hunt, 2005) indicates that even moderate volumes of retained particles, in the order of 1% of the porous volume, or lower, usually result in extremely pronounced clogging, causing an increase of pressure drops of two to three orders of magnitude. Clogging can be modeled through a reduction in permeability, due to a concurrent decrease of the pore space available for the fluid flow $\varepsilon(s)$, and an increase of the specific surface area of the liquid (pore water) - solid (matrix plus deposited particles) interface $a(s)$ (Tosco and Sethi, 2010):

$$\varepsilon(s) = n - \frac{\rho_b}{\lambda \rho_p} s \tag{2}$$

$$a(s) = a_0 + \theta\, a_p \frac{\rho_b}{\rho_p} s \tag{3}$$

where n is the porosity before the injection of the particles [-], a_0 is the specific surface area of the porous matrix in the absence of particle deposits [L^{-1}], a_p is the specific surface area of the nanoparticles [L^{-1}], ρ_p is the density of nanoparticles [$M\,L^{-3}$]. The parameter λ is the volume of the particles per unit volume of particle deposits [-], and consequently represents the degree of packing of the deposits. It can vary in the range $0<\lambda<1$: the higher λ, the more packed are the

deposits, and consequently the highest the overall density of the deposits, $\lambda \rho_p$. The parameter θ represents in turn the fraction of deposited nanoparticles contributing to the overall increase of the solid-liquid interface area [-], following Mays and Hunt (2005), with $0<\theta<1$, being θ higher for more irregular deposits. If the permeability coefficient $K(s)$ is assumed to depend on the third power of porosity and the square of the specific surface area (Kozeny, 1927), then it can be expressed as (Tosco and Sethi, 2010):

$$K(s) = K_0 \left[\frac{\varepsilon}{n} \right]^3 \left[\frac{a_0}{a} \right]^2 \tag{4}$$

where K_0 is the permeability coefficient in the absence of deposited particles [L^2].

It was observed that, during particle deposition, the most relevant contribution to permeability reduction (and consequently to clogging) is usually do to a significant increase in the specific surface area of the liquid-solid interface, rather than to porosity reduction (Mays ad Hunt, 2005). In transport column tests, the overall pressure drop between column entrance and exit, which can be measured by pressure sensors/gauges and directly related to the average degree of clogging of the column, corresponds to the space integral of Darcy law (at a certain time):

$$\Delta P(t) = P_{in}(t) - P_{out}(t) = -q \int_0^L \frac{\mu(x,t)}{K(x,t)} dx \tag{5}$$

where L is the column length [L] and $\mu(x, t)$ is the dynamic viscosity of the mobile phase in distance of x and time t [$ML^{-1}T^{-1}$]. The permeability is a time- and space-dependent variable (being function of s). As a general rule, also the fluid viscosity may be a time- and space-

dependent variable (Tosco and Sethi, 2010). However, in this work it was assumed to be a constant parameter, equal to water dynamic viscosity.

In this study, the software E-MNM1D (Tosco and Sethi, 2010) was used for direct and inverse simulation of the transport and retention behavior of the nano-*Fe/Cu* particles injected through sand columns. Two interaction sites were considered, following equation (1). Newtonian properties were assumed for both flushing water and *Fe/Cu* particle suspensions, neglecting effects of particle concentration on viscosity, $\mu_f = \mu_w$. The solution to equations (1) to (5) provided by E-MNNM1D assumes one-dimensional, horizontal, quasi-stationary flow, constant discharge, and negligible compressibility of particles, porous matrix, pore fluid, and particles deposits.

Initial conditions of zero concentration of particles in both liquid and solid phase were imposed. A homogeneous second type boundary condition was assumed at the column outlet ($x = L$). A fist type boundary condition was assumed at the inlet ($x = 0$), simulating a step injection of particles at a constant concentration C_0 for $0 \le t \le t_{inj}$, followed by a zero inlet concentration up to the end of the simulation ($t_{inj} \le t \le t_{inj} + t_{flush}$).

The equations are solved using a finite differences approach (Tosco and Sethi, 2009), with space and time steps respectively equal to $\Delta x = 0.0025$ m and $\Delta t = 2$ s. Sand column geometry (L and inner radius), porous medium characteristics (ρ_b, d_{50}, K, k, and n), properties of the nanoparticles (d_{50}, ρ_p, and SA), and influent water characteristics (μ, ρ_w) were assumed as known parameters (Table A1 in the Appendix section). Transport and clogging parameters, namely the deposition and release (detachment) parameters (k^1_a, k^2_a, k^1_d, k^2_d, A_1, β_1, and β_2) and the parameters controlling the clogging phenomena (λ and θ), were obtained from the inverse solution of the equations (1) to (5) using a least-squares procedure.

The inverse modeling was applied only on the three tests for $C_0 = 8$ g/l, thus providing three sets of model parameters, one for each considered flow rate (5×10^{-4}, 1×10^{-3}, 2×10^{-3} m/s). The inverse-fitted parameters were then used for the direct simulation of the other tests performed with $C_0 = 2$, 5 and 12 g/l. The duration of injection and flushing period (respectively, t_{inj} and t_{flush}) was the same for all simulations, namely $t_{inj} = 1050$ s and $t_{flush} = 5700$ s, for a total simulation time of 6750 s. The values of the transport and clogging parameters were determined by simultaneous fitting of the observed BTC of nanoparticles concentration (C_{obs}), pressure drop during time (ΔP_{obs}), and spatial distribution of retained nanoparticles concentration on the solid phase after the flushing period, to the corresponding simulated values:

$$\begin{cases} C(x=L,t) = C_{obs}(t) \\ S(x, t=t_{flush}) = S_{obs}(x) \\ \int_0^L p(x,t)dx = \Delta P_{obs}(t) \end{cases} \tag{12}$$

3. Results and Discussion

3.1. Tracer tests

To compare the transport behavior of an ideal solute (a tracer) with the NZVI through the used sand in the experiments, a series of tracer tests using *NaCl* were conducted. The normalized C/C_0 breakthrough curves of the tracer for the three velocities are shown as colored points in Figure (A1) in the Appendix section. Longitudinal dispersivity (α_L) of the medium was calculated from tracer BTCs at different flow rates using the analytical approach developed by Singh (2002) for

advective-dispersive transport of an ideal solute in homogeneous and isotropic porous media averagely equal to 5.7×10^{-3} m.

It is known that the effective velocity of a particle in a porous medium is higher than the one observed for water and solutes (Wood and Ehrlich, 1978; Toran and Palumbo, 1992). However, under some circumstances, the difference can be neglected, and effective velocity of a particle can be approximated with the values obtained from tracer tests. An estimate of this discrepancy can be obtained from the correlations proposed by Johnson and Elimelech (1995) and Di Marzio and Guttman (1970) for, respectively, the average pore size of the porous medium and the effective velocity of the NZVI particles flowing through it. For the particle size and flow rates used in this work, the discrepancy correlation suggests that the average pore diameter is 4.8×10^{-4} m and the ratio of colloid to water flow rate is 0.01%. These values are acceptably small to support the use of the parameters obtained from tracer tests to assess NZVI transport.

3.2. Transport tests of *Fe/Cu* nanoparticles: experimental results and numerical modeling

The observed BTCs of nanoparticles (C/C_0) as a function of time (Figure 1) in different experimental conditions of pore water velocities ($V = 5 \times 10^{-4}$, 1×10^{-3}, 2×10^{-3} m/s) and injected concentrations ($C_0 = 2, 5, 8,$ and 12 g/l) are presented in Figure (1) by open colored circles. The corresponding profiles of pressure drop over time (ΔP) are reported in Figure (2).

The breakthrough curves (Figure 1) indicate that both V and C_0 have a relevant impact on NZVI mobility, even if the influence of C_0 is more evident. In all experimental conditions, the BTCs are not symmetrical, which indicates that attachment and detachment phenomena are occurring in different modes. The observed profiles of pressure drop (ΔP) as a function of time

16

(Figure 2) indicate that in all of the 12 experiments, ΔP increased during the injection period (the maximum ΔP value was always observed at $t= t_{inj}$) and then declined during the flushing period. Because the viscosity of NZVI dispersion is the same as the viscosity of the water used for flushing (Table S1), it can be concluded that all the increase in pore pressure during injection is due to clogging phenomenon caused by deposited NZVI, with a consequent reduction in permeability.

Figure (1) and Figure (2) also report the simulated curves of C/C_0 and ΔP obtained from direct and inverse simulations in E-MNM1D. Three sets of model parameters (Table 1) were obtained from simultaneous inverse fitting of experimental breakthrough curves, pressure drop curves and profiles of deposited particle concentration for the tests performed injecting $C_0 = 8$ g/l. Each set of transport coefficients correspond to a different flow rate (5×10^{-4}, 1×10^{-3}, and 2×10^{-3} m/s). Model curves for tests with $C_0= 2$, 5 and 12 g/l, also reported in Figures (1) and (2), were instead obtained from direct simulations using the transport parameters obtained from the tests at $C_0 = 8$ g/l. As a general rule, experimental and model curves are in good agreement among them, both for inverse-simulated tests ($C_0= 8$ g/l) and for the others ($C_0= 2$, 5, and 12 g/l). The correlation coefficient (R^2) and also P-value statistic based on F-test (with $\alpha=0.05$) between the observed and simulated values of ΔP and C/C_0 to investigate the equality of variances have been calculated and shown in Table (A2) in the Appendix section. The calculated R^2 values have the range of 0.75 to 1.00, and the P-values have a significance level of 95% for most circumstances, except two cases of ΔP profiles, when $C_0=8$ g/l and $V=5\times10^{-4}$, 1×10^{-3}, and 2×10^{-3} m/s. A slightly more pronounced discrepancy can be noticed for the highest nanoparticles concentration, but overall the quantitative and qualitative agreement is satisfactory. Even if the transport coefficients were determined from inverse fitting of the experimental data of only one injected

concentration, the comparison of experimental and simulated curves for the other values of C_0 indicate that they can be considered independent on the injected concentration under identical flow rate. This finding is important in particular for the attachment and detachment coefficients, k^i_a and k^i_d: different inlet concentrations give rise to extremely different amounts of deposited particles, which may or may not result in clogging of the porous medium, depending on C_0, thus indicating that, in the deposition term of the second and third equations in (1), the concentration of suspended particles has a strong influence on the deposition process. An independence of attachment coefficients on the concentration of particles suspended in the pore water was expected, as input concentration has no effect on particle-collector interaction energies and deposition efficiency, On the other hand, an influence of C_0 could have been hypothesized during NZVI injection, but was not clearly observed in our results, probably due to the predominance of deposition phenomena, which masked changes in release rates with changing C_0.

The simulated and observed profiles of normalized retained particle concentration ($S/V.C_0$) along the column for C_0=8 g/l and different velocities (V= 5×10^{-4}, 1×10^{-3}, and 2×10^{-3} m/s) at two stages are shown in Figure (4), one at the end of injection period ($t=t_{inj}$=1050 s, Figure 4a to 4c) and another at the end of flushing period (t= 6700 s, Figure 6d). Simulated profiles for C_0 = 2, 5, and 12 g/l and different velocities (V) at t=6700 s are reported in Figure (A2) in the Appendix section. All profiles were normalized by the injected mass flux ($V.C_0$) to allow comparison of the tests performed at different flow rates (and therefore injecting different mass of particles, being the injection duration the same in all tests).

The influence of flow rate can be clearly observed in the profiles of deposited concentration. Increasing the pore water velocity through the column (Figure 4a compared to 4c) caused a reduction in deposition, which is consistent with the common behavior of colloidal nanoparticles

reported in the literatures (Wang, 2009; Tosco *et al.*, 2012). However, the shape of the deposits is the same for all flow rates, suggesting that *V* influences the amount of deposited particles, but not the deposition mechanism.

The mass balance of nano-*Fe/Cu* particles was determined by comparing the total weight of nanoparticles injected to the column during the t_{inj}, to the corresponding value obtained by sum of weight of effluent particles calculated from integrating the particle breakthrough curve (C/C_0) with the amount retained (deposited) particles (*S*) on the length of sand after flushing period for each pore water velocity. The mass balance was applicable only for condition of $C_0 = 8$ *g/l* and $V = 5 \times 10^{-4}$, 1×10^{-3}, and 2×10^{-3} *m/s* due to availability of observed values of deposited particles. Results of mass balance calculation summarized in Table (2). The mass balance was found to be $\pm 1.0\%$, $\pm 4.5\%$, and $\pm 24.1\%$, respectively for $V = 5 \times 10^{-4}$, 1×10^{-3}, and 2×10^{-3} *m/s* which reveals that increasing in *V* corresponds to smaller variability to calculate the mass balance.

3.3. Mechanisms of particle deposition and release

Deposition during nanoparticle injection is more evident for low flow rates, and high injected concentrations C_0. This is consistent with the literature for colloid transport in general (Cullen *et al.*, 2010), and for iron-based nanoparticles in particular (Dalla Vecchia *et al.*, 2009b; Tosco *et al.*, 2012). The fitted inverse-values of deposition and release coefficients for both sites (k^i_a and k^i_d) coherently indicate a moderate dependence on flow rate: attachment coefficients decrease with increasing flow rate, while detachment coefficients increase with increasing flow rate. The shape of the breakthrough curves in the advanced stages of deposition suggests that a dynamic equilibrium between deposition and release is not reached during NZVI injection. In all tests, except those for the lowest C_0 (Figure 1a), the BTCs, after the initial increase, showed a strong

decline, which is a clear indication of ripening (Li *et al.*, 2005; Tosco and Sethi, 2010). This phenomenon became more evident with increasing the injected concentration. Ripening is modeled by positive inverse-fitted values of the parameter A_1 (Table 1), which is only moderately affected by the flow rate. Whereas, the negative and zero value of A_1, respectively indicate the blocking phenomenon and linear isotherm. Ripening is also consistent with the non linear increase in pressure drop curves for the highest injected concentrations C_0.

Further analysis of the breakthrough curves show that release during flushing increased mainly with increasing the injected concentration C_0, while flow rate had a minor impact. For the lowest C_0, the decline of the BTCs at the beginning of flushing was abrupt, regardless the flow rate. For $C_0= 5$ *g/l* (Figure 1b), a slight retarded decline of breakthrough concentration was observed, suggesting that a fraction of the deposited particles were released. Further increasing the injected concentration (Figures 1c and 1d), a multi-modal behavior was observed (see colored arrows). At the early stages of flushing, a first rapid release was registered (blue arrows), while a second, delayed peak was observed during advanced flushing (red arrows). This suggests that two different release mechanisms are occurring for $C_0= 8$ and 12 *g/l* at the three pore water velocities, one associated with fast detachment of particles retained in Site 1 ($k^1_d = 0.016$, 0.032, and 0.039, respectively for $V= 5\times10^{-4}$, 1×10^{-3}, and 2×10^{-3} *m/s*) and a second associated with slow detachment of colloids retained on Site 2, which is characterized by detachment coefficients of approximately one order of magnitude lower than those of Site 1 ($k^2_d = 0.003$, 0.002, and 0.003, respectively for $V=5\times10^{-4}$, 1×10^{-3}, and 2×10^{-3} *m/s*). It seems that this behavior is associated to the value of C_0, rather than to the pore water velocity, as the flow rate affected the position of the second peak, but did not have a relevant influence on its height and shape.

The profiles of retained particles at the end of injection time ($t=t_{inj}$) decreases in nonlinear form with increasing distance from the $x=0$ (Figure 4a to 4c), whereas conversely the retained profiles at the end of flushing step, increases with distance (Figure 4d). This inverse behavior of deposited particles at two times of $t=t_{inj}$ and $t= t_{inj}+ t_{flush}$ are corresponding to the variation of the particles attachment and detachment behavior at sites of s_1 and s_2 as shown in Figure (Figure 5a to 5d). For the injection period, the deposited particles at s_1 is at least 10 times greater than those at s_2 (Figure 5a and 5c) for each distance of x. In the other words, during the injection period, the physical-chemical interaction which is modeled at s_1 is dominated for particle attachment and the straining kinetics is limited. In addition, increasing the pore water velocity (V) lead to larger variation of deposited particles along the column for both sites. Similar condition is also observed during the flushing period, as the space-dependent dynamics which follows at s_2, is predominated by the process modeled by the s_1 for the particle detachment (Figure 5b and 5d). At flushing period, the pore water velocity (V) has a greater effect on the particle detachment than particle attachment for both sites. Since the shapes of all figures are similar, the flow rate (V) influences the amount of deposited particles in two sites, but not the deposition mechanism.

It is concluded that since the rate of attachment and detachment processes associated to the s_2 is slower than to the s_1, deposition for both sites was found to be (almost) completely reversible. The experimental profiles of concentration of deposited particles, measured at the end of the column tests (that is, at the end of flushing with particle-free water), exhibit a negligible concentration at the column entrance, and an increasing concentration with increasing distance from column inlet, which is not often reported in the literature. This result indicates that, when the tests were stopped, the release process was not totally completed along the entire column (which can also be observed in breakthrough curves, not reaching zero outlet concentration at the

end of the tests). When the profiles were measured, particles reversibly deposited close to column inlet had already been detached from the porous medium, resulting in extremely low residual concentrations, while detachment was not complete in the sections of the column closer to the outlet. This finding is a confirmation of the hypothesis of reversible deposition on both interaction sites: in case of irreversible deposition, the concentration of deposited particles should have been higher at column inlet, decreasing along the column as observed in the Figure (4a to 4c) at $t=t_{inj}$.

3.3. Porous medium clogging

The occurrence of clogging during particle injection is particularly evident in the plots of pressure drop ΔP over time (Figure 2) for the tests performed at high injected concentration. Combined analysis of breakthrough curves (Figure 1) and pressure curves (Figure 2) provides information on the deposition and release mechanisms. At the lowest injected concentration $C_0=$ 2 and 5 g/l (Figure 2a and 2b), no significant clogging was observed. The pressure drop stayed almost constant during the entire test and was clearly controlled by the flow rate. Doubling the flow rate resulted in doubling the pressure drop, that is, a linear dependence is observed, following Darcy law (compare for example the test for $V= 5 \times 10^{-4}$, 1×10^{-3}, and 2×10^{-3} m/s in Figure 2a).

For higher values of C_0, a peak in the pressure plot was registered, which became more and more pronounced with increasing C_0 (Figure 2b to 2d). This peak can be attributed to clogging. The combined effect of ΔP due to flow and ΔP due to clogging is particularly evident when comparing the results for tests with $C_0 = 2$ g/l (Figure 2a) and $C_0= 5$ g/l (Figure 2b). When further increasing C_0 (Figures 2c and 2d), the contribution to pressure drop due to clogging increased

dramatically, coherently with the strong ripening observed in the breakthrough curves (Figure 1c and 1d). For a better comparison, the measured maximum pressure drop (ΔP) versus pore water velocity (V) at $t=t_{inj}$, for different injection of nanoparticle (C_0) is shown as semi-logarithmic in Figure (3). The peak pressure increases linearly with flow rate, coherently with Darcy law, while changes in injected concentration resulted in changes of peak pressure of orders of magnitude. This finding supports the direct relationship between concentration of deposited particles and pressure drop, which is included in the transport model (Equations 2 to 5).

Clogging is simulated through a reduction in porosity and permeability. The controlling parameters are the coefficients λ and θ, which result to be moderately affected by flow rate (Table 1). In particular, clogging can also be related to changes in the averaged effective porosity (AEP), which can be calculated as the integral of space-dependent porosity along the column:

$$AEP(t) = \frac{1}{L} \int_0^L \varepsilon(x,t)dx \qquad (7)$$

To better follow the variations of AEP over time, and also investigate the time that AEP profiles restore to the initial values (0.37) in different conditions, the simulation flushing period in EMNM1D code was extended up to 35,000 s to better follow the AEP variation during time (Figure 6). Obtained results can be briefly state as follows:

1) AEP reduction is affected by a combination of both V and C_0, with colloid concentration dominating over the effect of V, and

2) the time at which maximum AEP reduction occurs is earlier for conditions of high C_0 (all conditions in Figure 6d) and high V (green lines in Figure 6a to 6d) because at high input colloid

concentrations ripening occurs, and at high velocities the stagnant zone volume in the porous medium is minimal.

4. Conclusions

Results of this study show that using copper as partial coating metal onto the NZVI surface promotes the colloidal stability of the particle slurries when they are injected in the saturated coarse sand columns. Transport and retention mechanisms of highly concentrated nano-*Fe/Cu* particles (2-12 *g/l*) through high flow-rated sand column were simulated as well by the numerical modeling of modified advection-dispersion-deposition equation by E-MNM1D. Both experimental and modeling results show that bimetallic nano-*Fe/Cu* particles can be injected, easily and transported without significant retention in the sand medium and also decrease in effective porosity through column. The transport tests also indicated that the injected concentration has an extremely relevant impact on the injectability of the particles. Injected concentrations in the order of 8 *g/l* or higher gave rise to pronounce clogging phenomena, which could have a negative impact on a field injection of the particles, both in terms of mobility in the subsurface and injection pressure required. Clogging seemed to be caused by ripening deposition dynamics, and mainly controlled by the injected concentration, while flow rate had a minor impact.

In the efforts of guiding the design of environmental remediation strategies for a specific contaminated site prior to deployment, this study provides valuable information on the transport behavior of nano-*Fe/Cu* ex-situ for the chemical conditions encountered in the field (specially for Karaj aquifer). Future improvements to the reactive transport models on which environmental remediation strategies are based should consider including: i) long-term reaction kinetics of the particles with their target contaminant, and ii) dispersal of the injected nanoparticles outside the

boundaries of the affected area to minimize potential adverse effects on ecosystem and public health.

5. Appendix A: Supporting Information

Supporting information section is provided to indicate the more information about the parameter values used in numerical modeling (Table A1), statistical criteria (R^2 and P-value) between the observed and simulated values of ΔP and C/C_0 (Table A2), observed and fitted BTC curves of tracer tests through the sand column (Figure A1), and simulated normalized retained particle concentration profiles at the end of transport test (Figure A2).

6. References

Bear, J., 1979. Hydraulics of Groundwater, McGraw-Hill Pub Co.

Bhattacharjee, S., Ryan, J.N., and Elimelech, M., 2002.Virus transport in physically and geochemically heterogeneous subsurface porous media. Journal of Contaminant Hydrology, 57,161–87.

Bradford, S.A., and Torkzaban, S., 2008. Colloid transport and retention on in unsaturated porous media, a review of interface-, collector-, and pore-scale processes and models. Vadose Zone Journal, 72, 667–681.

Bradford, S.A., Simunek, J., Bettahar, M., van Genuchten, M.T., and Yates, S.R., 2003. Modeling colloid attachment, straining, and exclusion in saturated porous media. Environmental Science and Technology, 37, 2242-2250.

Caldelas, F.M., 2010. Experimental parameters analysis of nanoparticle retention in porous media.Thesis of Master of Science in Engineering, Faculty of Graduate School of University of Texas of Austin.

Cantrell, K.J., Kaplan, D.I. and Gilmore, T.J., 1997.Injection of colloidal Fe0 particles in sand with shear thinning fluids. Journal of Environmental Engineering, 123, 786–791.

Cullen, E., O'Carroll, D.M., Yanful, E.K., and Sleep, B., 2010.Simulation of the subsurface mobility of carbon nanoparticles at the field scale. Advances in Water Resources, 33, 361–371.

Dalla Vecchia, E., Coisson, M., Appino, C., Vinai, F., Sethi, R., 2009. Magnetic characterization and interaction modeling of zerovalent iron nanoparticles for the remediation of contaminated aquifers. J. Nanosci. Nanotech. 9 (5) , 3210-3218.

DallaVecchia, E., Luna, M., and Sethi, R., 2009. Transport in Porous Media of Highly Concentrated Iron Micro- and Nanoparticles in the Presence of Xanthan Gum. Environ. Sci. Technol., 43 23, 8942–8947.

DiMarzio, E.A., Guttman, C.M., 1970. Separation by Flow. Macromolecules 32, 131-146. doi,10.1021/ma60014a005.

Dobrinas, S., Soceanu, A., Gheorghiu, C.B. and Tanase, M., 2010. Comparative methods applied for the determination of total iron from beer samples. Ovidius University Annals of Chemistry, 211, 35-40.

Elliott, D.W., and Zhang, W.X., 2001.Field assessment of nanoscale bimetallic particles for groundwater treatment. Environ. Sci. Technol., 35, 4922–4926.

Freeze, R.A. and Cherry, J.A., 1979.Groundwater, Prentice Hall, Inc.

Freyria, F.S., Bonelli, B., Sethi, R., Armandi, M., Belluso, E., Garrone, E., 2011. Reactions of acid orange 7 with iron nanoparticles in aqueous solutions. Journal of Physical Chemistry C 115 (49) , 24143-24152.

Gillham, R.W., Ohannesin, S.F. (1994). Enhanced degradation of halogenated aliphatics by zero-valent iron. Ground Water 32(6), 958-967

Grolimund, D., and Borkovec, M., 2006. Release of colloidal particles in natural porous media bymonovalent and divalent cations. J. Contaminat.Hydrol., 87, 155-175.

Haan, C.T., 2002. Statistical methods in hydrology. Second Edition, Iowa State Press, pp. 496.

Hamby, D.M., 1994. A Review of Techniques for Parameter Sensitivity Analysis of Environmental Models. Environmental Monitoring and Assessment, 32, 135-154.

He, F., and Zhao, D., 2005. Preparation and characterization of a new classof starch-stabilized bimetallic nanoparticles for degradation ofchlorinated hydrocarbons in water. Environ. Sci. Technol., 39, 3314–3320.

Hee, K.Sh., and Cha, D.K., 2008. Microbial reduction of nitrate in the presence of nanoscale zero-valent iron.Chemosphere, 72 2, 257-262.

Helton, J.C., Iman, R.L. and Brown, J.B., 1985. Sensitivity Analysis of the Asymptotic Behavior of a Model for the Environmental Movement of Radionuclides, Ecological Modelling, 28, 243-278.

Hosseini, S.M., Ataie-Ashtiani, B., and Kholghi, M., 2011. Nitrate reduction by nano-Fe/Cu particles in packed column, Desalination., 276, 214-221. doi,10.1016/j.desal.2011.03.051.

Hosseini, S.M., Kholghi, M., and Vagharfard, H., 2012. Numerical and meta-modeling of nitrate transport reduced by nano-Fe/Cu particles in packed sand column, Transp Porous Med Accepted, DOI 10.1007/s11242-012-9994-z.

Iman, R.L., and Helton, J.C., 1988. An Investigation of Uncertainty and Sensitivity Analysis Techniques for Computer Models. Risk Analysis, 8, 71-90.

Jaisi, D.P., Saleh, N.B., Blake, R.E., and Elimelech, M., 2008. Transport of single-walled carbon nanotubes in porous media, filtration mechanisms and reversibility. Environ. Sci. Technol., 4222, 8317–23.

Johnson, P.R., Elimelech, M., 1995. Dynamics of Colloid Deposition in Porous-Media - Blocking Based on Random Sequential Adsorption. Langmuir 113, 801-812.

Kanel, S.R,Goswami, R.R., Clement, T.P., Barnett, M.O., and Zhao, D., 2008. Two Dimensional Transport Characteristics of Surface Stabilized Zero-valent Iron Nanoparticles in Porous Media. Environ. Sci. Technol., 42 (3), 896–900.

Kanel, S.R., Nepal, D., Manning, B., and Choi H., 2007. Transport of surface-modified iron nanoparticle in porous media and application to arsenicIII remediation. J Nanopart Res, 9,725–735.

Kim, S.C., Harrington, M.S., and Pui, D.Y.H., 2007.Experimental study of nanoparticles penetration through commercial filter media, Journal of Nanoparticle Research, 9,117–125.

Kozeny, J., 1927. Uber Kapillare Leitung des Wasser im Boden. Sitzungsberichte der Akademie der Wissenschaften Wien 136, 106-271.

Li, X., Zhang, P., Lin, C.L., Johnson, W.P., 2005. Role of Hydrodynamic Drag on Microsphere Deposition and Re-entrainment in Porous Media under Unfavorable Conditions. Environ, Sci. Technol., 3911, 4012-4020.

Li, Y.S., Wang, Y.G., Pennell, K.D., and Abriola, L.M., 2008. Investigation of the transport and deposition of fullerene C60 nanoparticles in quartz sands under varying flow conditions. Environ Sci Technol, 4219, 7174–80.

Liou, Y.H., Lo, S.L., Lin, Ch.J., Kuan, W.H., and Weng, Sh.Ch., 2005. Chemical reduction of an unbuffered nitrate solution using catalyzed and uncatalyzed nanoscale iron particles. Journal of Hazardous Materials, 127, 102–110.

Liu, Y.Q., Choi, H., Dionysiou, D., Lowry, G.V., 2005. Trichloroethenehydrodechlorination in water by highly disordered monometallic nanoiron. Chemistry of Materials 1721, 5315-5322. doi, 10.1021/Cm0511217

Mays, D.C., Hunt, J.R., 2005. Hydrodynamic aspects of particle clogging in porous media. Environmental Science & Technology, 392, 577-584

McCuen, R.H., 2003. Modeling hydrologic change, Statistical methods. Lewis Publishers, pp. 433.

Noubactep, Ch., Care, S., and Crane, R., 2011. Nanoscale metallic iron for environmental remediation, prospects and limitations. Water Air Soil Pollution Journal, DOI 10.1007/s11270-011-0951-1.

Otterstedt, J., and Brandreth, D.A., 1998. Small Particles Technology, Plenum Press, New York.

Phenrat, T., Cihan, A., Kim, H.-J., Mital, M., Illangasekare, T., and Lowry, G. V., 2010. Transport and deposition of polymer-modified Fe0 nanoparticles in 2-D heterogeneous porous media, Effects of particle concentration, Fe0 content, and coatings. Environ. Sci. Technol., 44 23, 9086–9093.

Phenrat, T., Kim, H.J., Fagerlund, F., Illangasekare, T., Tilton, R.D., and Lowry, G.V., 2009. Particle Size Distribution, Concentration, and Magnetic Attraction Affect Transport of Polymer-Modified Fe0 Nanoparticles in Sand Columns. Environ. Sci. Technol., 43, 5079–5085.

Phenrat, T., Saleh, N., Sirk, K., Tilton, R. D., and Lowry, G. V., 2007. Aggregation and sedimentation of aqueous nano scale zero valent iron dispersions. Environ. Sci. Technol., 41 1, 284- 290.

Saleh, N., Kim, H.-J., Phenrat, T., Matyjaszewski, K., Tilton, R.D., and Lowry, G. V., 2008. Ionic Strength and Composition Affect the Mobility of Surface-Modified Fe0 Nanoparticles in Water-Saturated Sand Columns. Environ. Sci. Technol., 42 9, 3349–3355.

Saleh, N., Sirk, K., Liu, Y., Phenrat, T., Dufour, B., Matyjaszewski, K., Tilton, R.D., and Lowry, G.V., 2007. Surface modifications enhance nanoiron transport and NAPL targeting in saturated porous media. Environ. Eng. Sci., 241, 45–57.

Singh, V.P., 2002, Kinematic wave solutions for pollutant transport over an infiltrating plane with finite-period mixing and mixing zone. Hydrological Processes 1612, 2441-2477.

Sun, N., Elimelech, M., Sun, N.Z., and Ryan, J.N., 2001.A novel two-dimensional model for colloid transport in a physically and geochemically heterogeneous porous media. Journal of Contaminant Hydrology, 49,173–99.

Sun, Y.P., Li, X.Q., Zhang, W.X., Wang, H.P., 2007. A method for the preparation of stable dispersion of zero-valent iron nanoparticles. Colloids and Surfaces A, Physicochemical and Engineering Aspects 3081-3, 60-66.

Tian, Y., Gao, B., Silvera-Batista, C., and Ziegler, K.J., 2010. Transport of engineered nanoparticles in saturated porous media, Journal of Nanoparticle Researches, DOI 10.1007/s11051-010-9912-7.

Tiraferri, A., Chen, K.L., Sethi, R., and Elimelech M., 2008. Reduced aggregation and sedimentation of zero-valent iron nanoparticles in the presence of guar gum. Journal of Colloid and Interface Science, 324, 71–79.

Tiraferri, A., Sethi, R., 2009. Enhanced Transport of Zerovalent Iron Nanoparticles in Saturated Porous Media by Guar Gum. Journal of Nanoparticle Research, 113, 635-645.

Tiraferri, A., Tosco, T., Sethi, R., 2011. Transport and retention of microparticles in packed sand columns at low and intermediate ionic strengths: Experiments and mathematical modelling. Environmental Earth Sciences, 63 (4) , 847-859.

Toran, L., Palumbo, A.V., 1992. Colloid transport through fractured and unfractured laboratory sand columns. Journal of Contaminant Hydrology 93, 289-303.

Tosco, T., and Sethi, R., 2010. Transport of non-newtonian suspensions of highly concentrated micro and nano scale iron particles in porous media, a modeling approach. Environ. Sci. Technol., 44, 9062–9068.

Tosco, T., Bosch, J., Meckenstock, R., Sethi, R., 2012. Transport of ferrihydrite nanoparticles in saturated porous media, role of ionic strength and flow rate. Environmental Science & Technology.doi,10.1021/es202643c

Tosco, T., Sethi, R., 2009. MNM1D, a numerical code for colloid transport in porous media, implementation and validation. American Journal of Environmental Sciences 54, 517-525

Tosco, T., Tiraferri, A., and Sethi, R., 2009. Ionic strength dependent transport of microparticles in saturated porous media, modeling mobilization and immobilization phenomena under transient chemical conditions. Environ. Sci. Technol., 43 12, 4425–4431.

Tratnyek, P.G., and Johnson, R.L., 2006.Nanotechnologies for environmental cleanup. Nano Today, 1 (2), 44–48.

Tratnyek, P.G., Scherer, M.M., Johnson, T.J., and Matheson, L.J., 2003.Permeable reactive barriers of iron and other zero-valent metals. In, Chemical Degradation Methods for Wastes

and Pollutants, Environmental and Industrial Applications, Tarr, M. A., Ed., Marcel Dekker, New York, 371-421.

Tufenkji, N., and Elimelech, M., 2004 a.Deviation from the classical colloid filtration theory in the presence of repulsive DLVO interactions. Langmuir, 20,10818-10828.

Tufenkji, N., and Elimelech, M., 2004 b. Correlation equation for predicting single-collector efficiency in physicochemical filtration in saturated porous media. Environ. Sci. Technol., 38, 529–536.

Wan, C., Chen, Y.H., and Wei, R., 1999.Dechlorination of chloromethanes on iron and palladium-iron bimetallic surface in aqueous systems. Environmental Toxicology and Chemistry., 18, 1091–1096.

Wang, R.K., Chen, W.C., Campos, D.K., and Ziegler, K.J., 2008.Swellingthe micelle core surrounding single-walled carbon nanotubes with water-immiscible organic solvents. J Am ChemSoc, 130,16330–16337.

Wang, Y., 2009. Transport and Retention of Fullerene-based Nanoparticles in Water Saturated Porous Media.Ph.D Thesis In Georgia Institute of Technology, pp., 235.

Wood, W.W., and Ehrlich, G.G., 1978. Use of Baker's Yeast to Trace Microbial Movement in Ground Water. Ground Water 166, 398-403. doi,10.1111/j.1745-6584.1978.tb03253.x.

Yang, G. C. C., and Lee, H. L., 2005. Chemical reduction of nitrate by nanosized iron, kinetics and pathways. Water Research, 39, 884–894.

Zanetti, M.C., Fiore, S. (2005). Evaluation of mutual connections between zero-valent iron reactivity and groundwater composition in trichloroethylene degradation. Annali di Chimica 95(11-12), 779-789.

Zhang, J., Zheng, T., Piringer, G., Day, C., McPherson, G. L., Lu, Y., Papadopoulos, K., and John, V. T., 2009. Transport characteristics of nanoscale functional zerovalent iron/silica composites for in situ remediation of trichloroethylene. Environ. Sci. Technol., 42 23, 8871–8876.

Zhang, W.X., 2003. Nanoscale Iron Particles for Environmental Remediation, An Overview. J. Nanopart. Res., 5, 323–332.
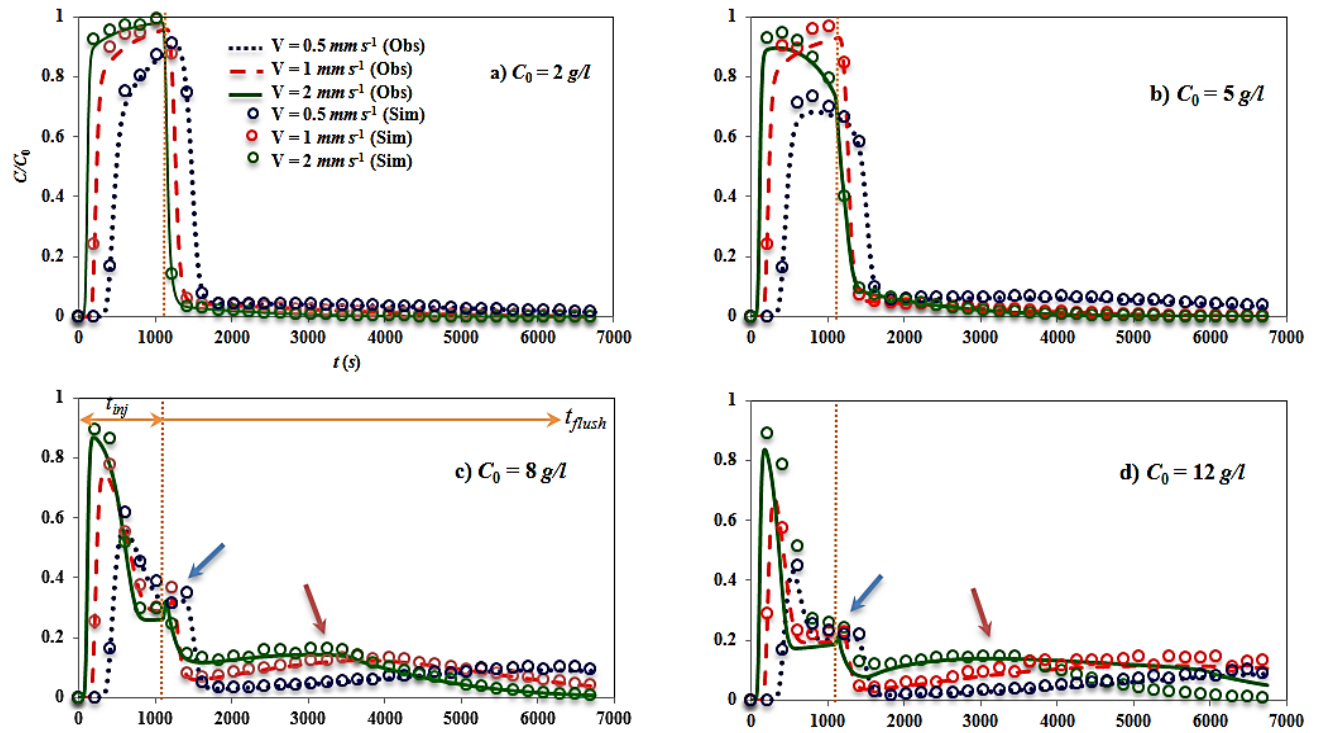
Figures

Figure (1): Effects of pore water velocity (*V*) and injected nanoparticle concentration (C_0) on the normalized NZVI breackthrough curves C/C_0. Colored symbols and lines indicate the observed and simulated values, respectively. The orange dotted lines indicate the end of the injection period.
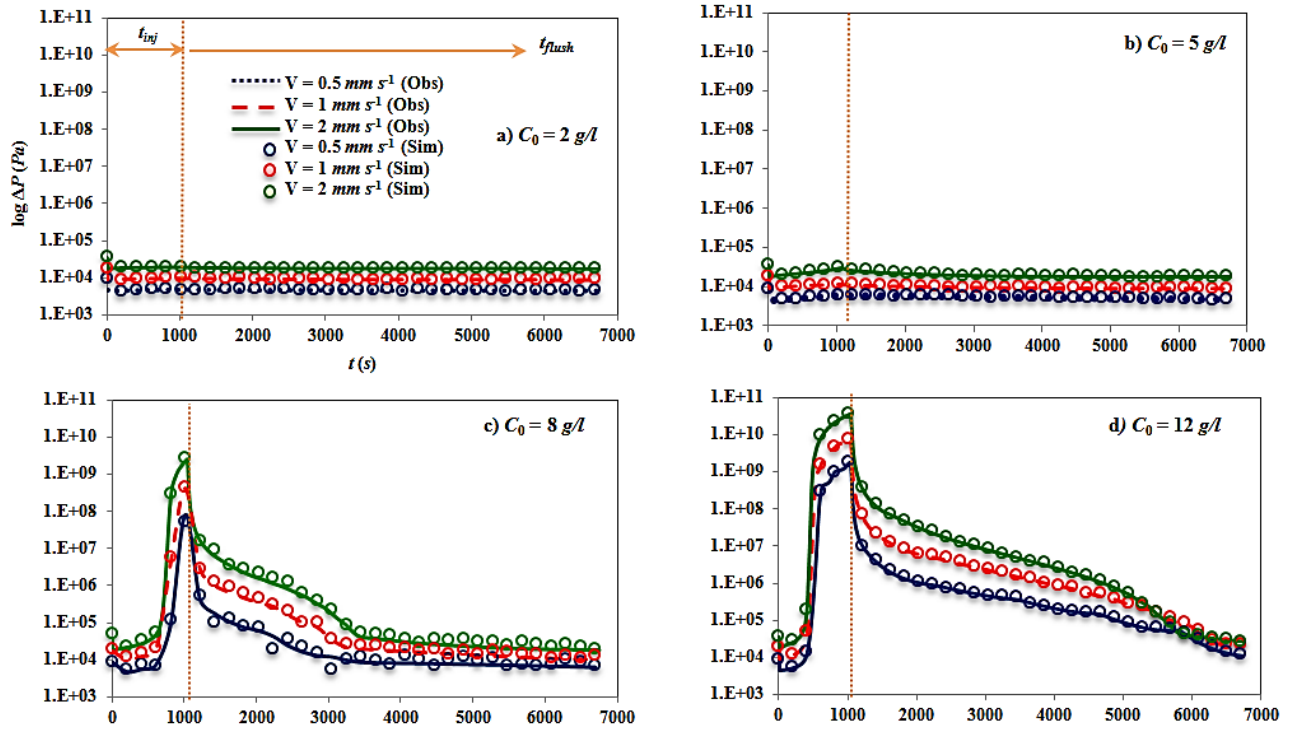
Figure (2): Effects of pore water velocity and (V) nanoparticle concentration (C_0) on the pressure drop of water (ΔP) through the column. Colored symbols and lines demonstrate the observed and simulated values, respectively.
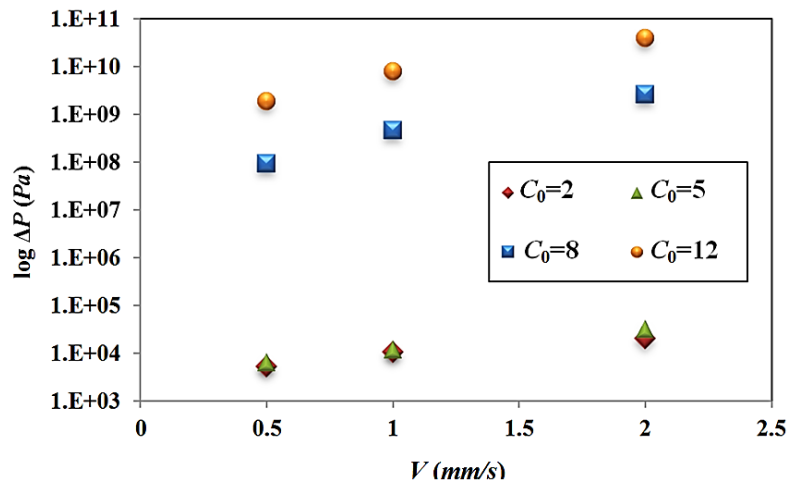

Figure (3): Peak pressure drop ΔP versus V for different injection concentrations of nanoparticles (C_0). Results are corresponding to the time of $t = t_{inj}$.
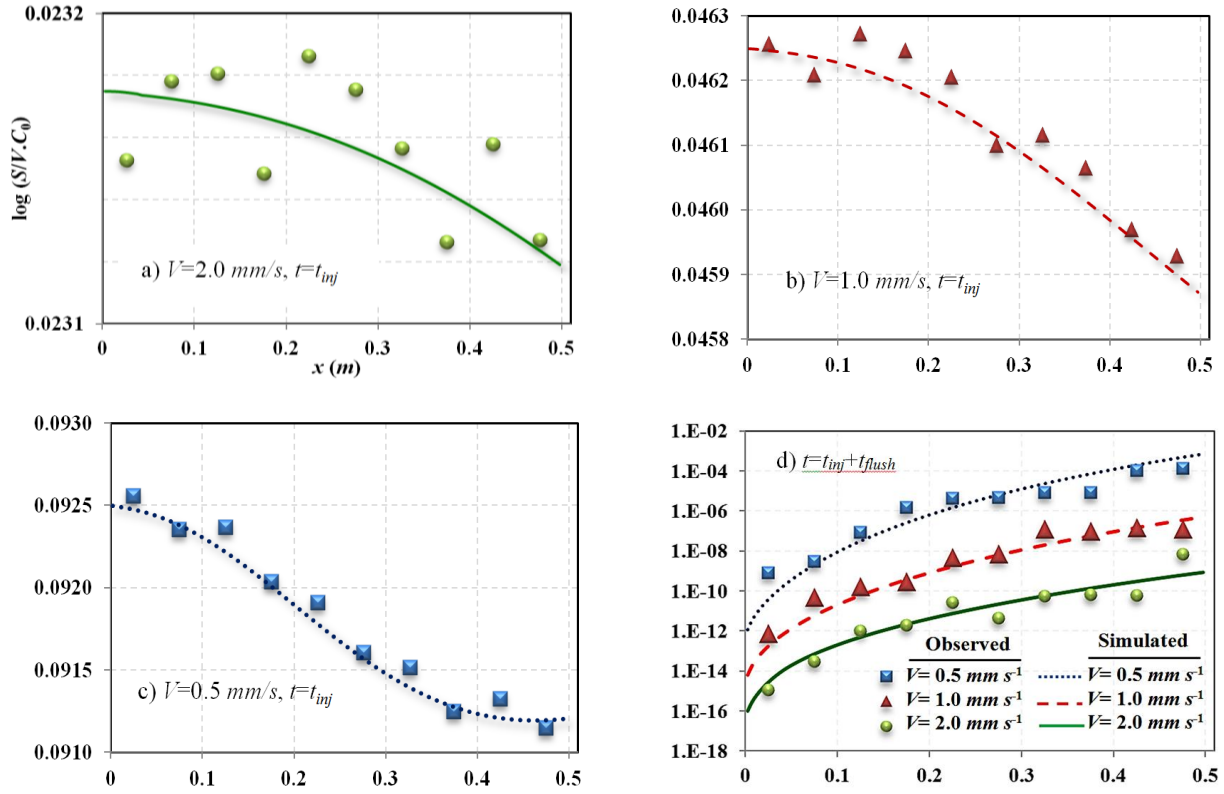
Figure (4): Normalized retained particle concentration profiles for $C_0 = 8$ *g/l* and different velocities. Figures (a) to (c) correspond to time at $t=t_{inj}$, and (d) at $t=t_{inj}+t_{flush}$. Experimental observations are presented as symbols, while simulations are presented as lines.
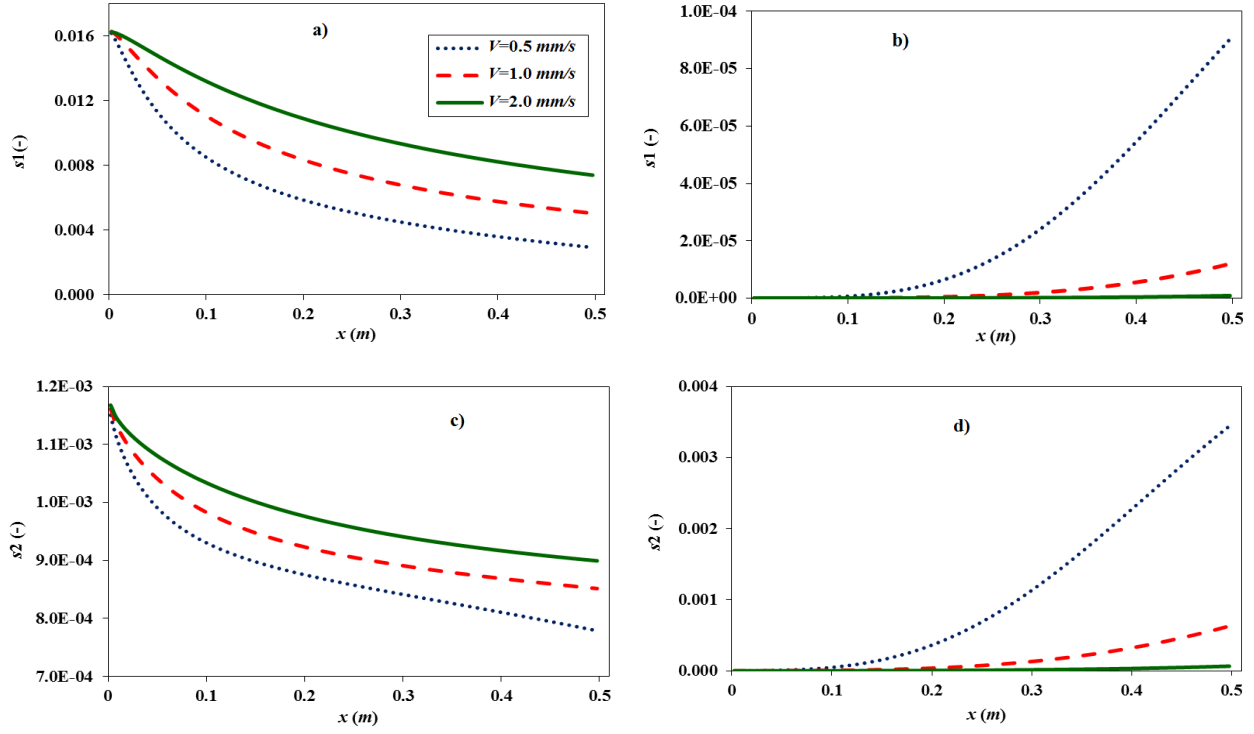
Figure (5): Development of the particle concentration in solid phase at site of s1 and s2 over space, for different velocities: (a and b) at the end of injection period, and (c and d) at end of flushing period (for all figures, $C_0=8$ *g/l*).
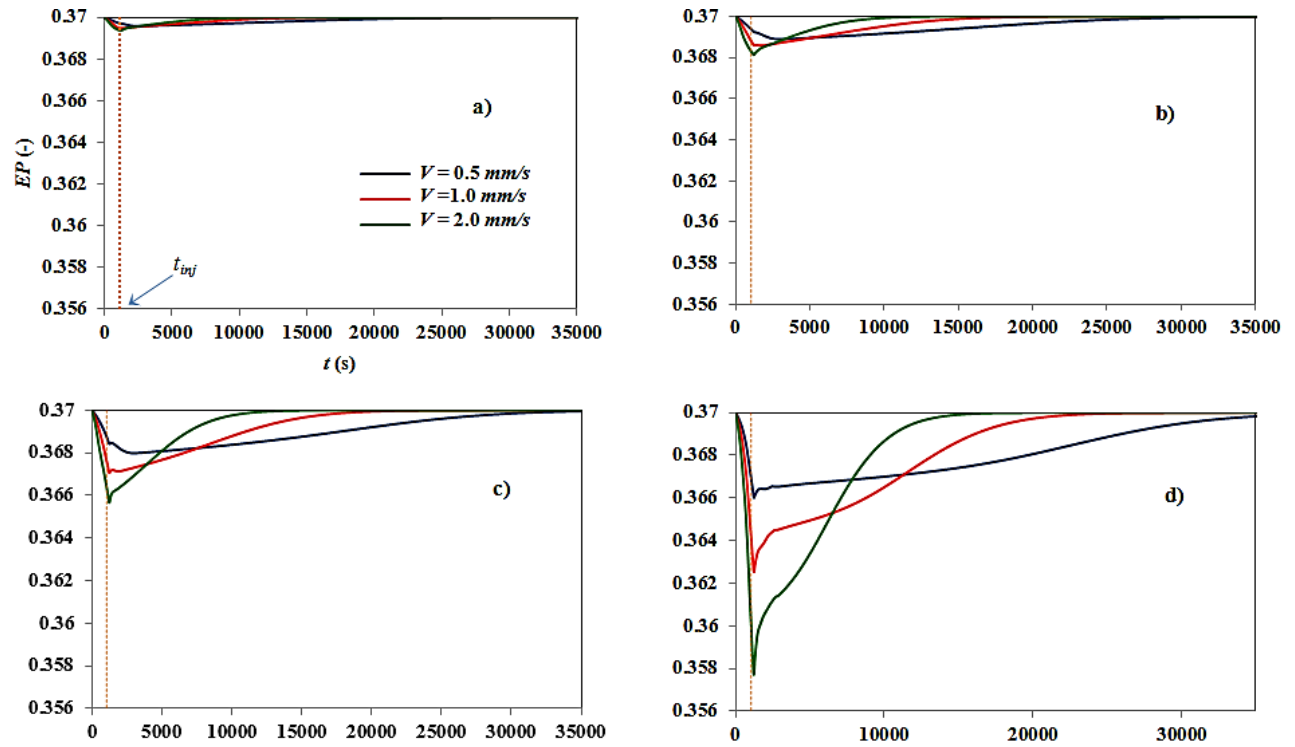
Figure (6): Effect of pore water velocity (V) and injected nanoparticle concentration (C_0) on the simulated average effective porosity (AEP) of the sand along the column during time: a) $C_0 = 2g/l$, b) 5 g/l, c) 8g/l and d) 12g/l.

Tables

Table (1): Fitted parameters values of the model parameters for different pore water velocity.

Parameter (unit)	Parameter Explanation	Fitted value[*]		
		$V=0.5$ mm/s	$V=1$ mm/s	$V=2$ mm/s
λ (-)	Average degree of packing of the particle deposits	0.371	0.354	0.354
θ (-)	Fraction of deposited nanoparticles contributing to the overall increase of the interface area	0.0036	0.0038	0.0050
k^1_a (s^{-1})	Deposition rate coefficients for the interaction site 1	0.0060	0.0128	0.0130
k^1_d (s^{-1})	Release rate coefficients for the interaction site 1	0.016	0.032	0.039
k^2_a (s^{-1})	Deposition rate coefficients for the interaction site 2	0.042	0.028	0.024
k^2_d (s^{-1})	Release rate coefficients for the interaction site 2	0.0030	0.0020	0.0032
A_1 (-)	Multiplier coefficients defining the interaction dynamics for site 1	3300	3685	4000
β_1 (-)	Exponent coefficients defining the interaction dynamics for site 1	1.460	1.485	1.510
β_2 (-)	Exponent coefficients defining the interaction dynamics for site 2	0.001	0.012	0.170

[*] In all three cases: $C_0 = 8$ g/l.

Table (3): Calculation of mass balance for nano-*Fe/Cu* particles in condition of C_0=8 g/l and V= 0.5, 1, and 2 mm/s.

Abbreviation	Component (unit)	V (mm/s)		
		0.5	1.0	2.0
C_1	Total injected Particle during t_{inj} (kg/m^3)	8400	16800	33600
C_2	Observed effluent particles from BTC of C/C_0 (kg/m^3)	6132.1	15960.0	33264.6
C_3	Observed deposited particles on sand after t_{flush} (kg/m^3)	239.3	83.2	22.5
Divergence (%)=$[C_1-(C_2+C_3)/C_1]\times100$		±24.1	±4.5	±1.0

Appendix A. Supporting Information

Supporting information section is provided to indicate the more information about the parameter values used in numerical modeling (Table A1), statistical criteria (R^2 and P- value) between the observed and simulated values of ΔP and C/C_0 (Table A2), observed and fitted BTC curves of tracer tests through the sand column (Fig. A1), and simulated normalized retained particle concentration profiles at the end of transport test (Fig. A2).
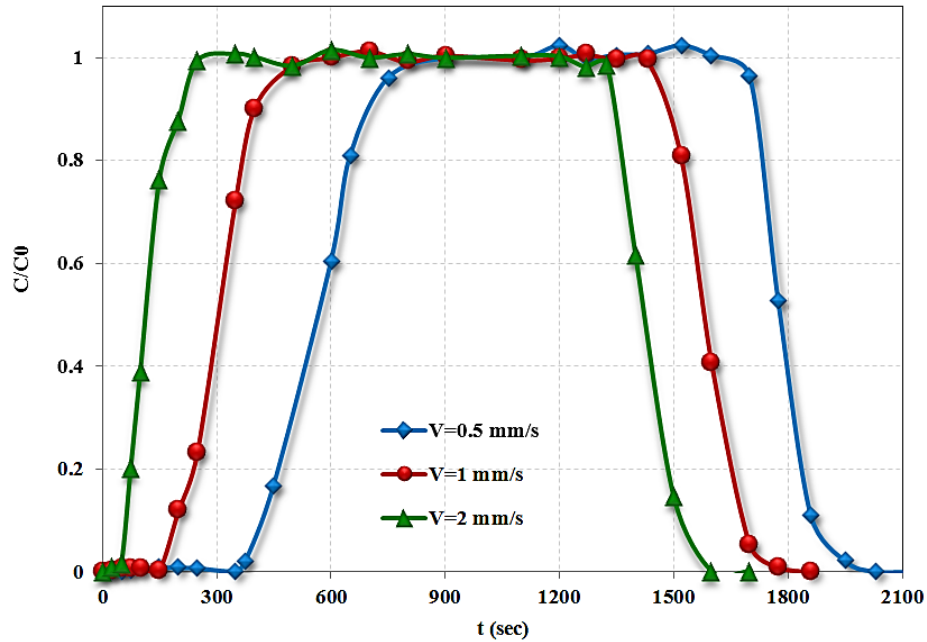

Figure (A1): Measured *NaCl* BTC curves as tracer in different pore water velocity
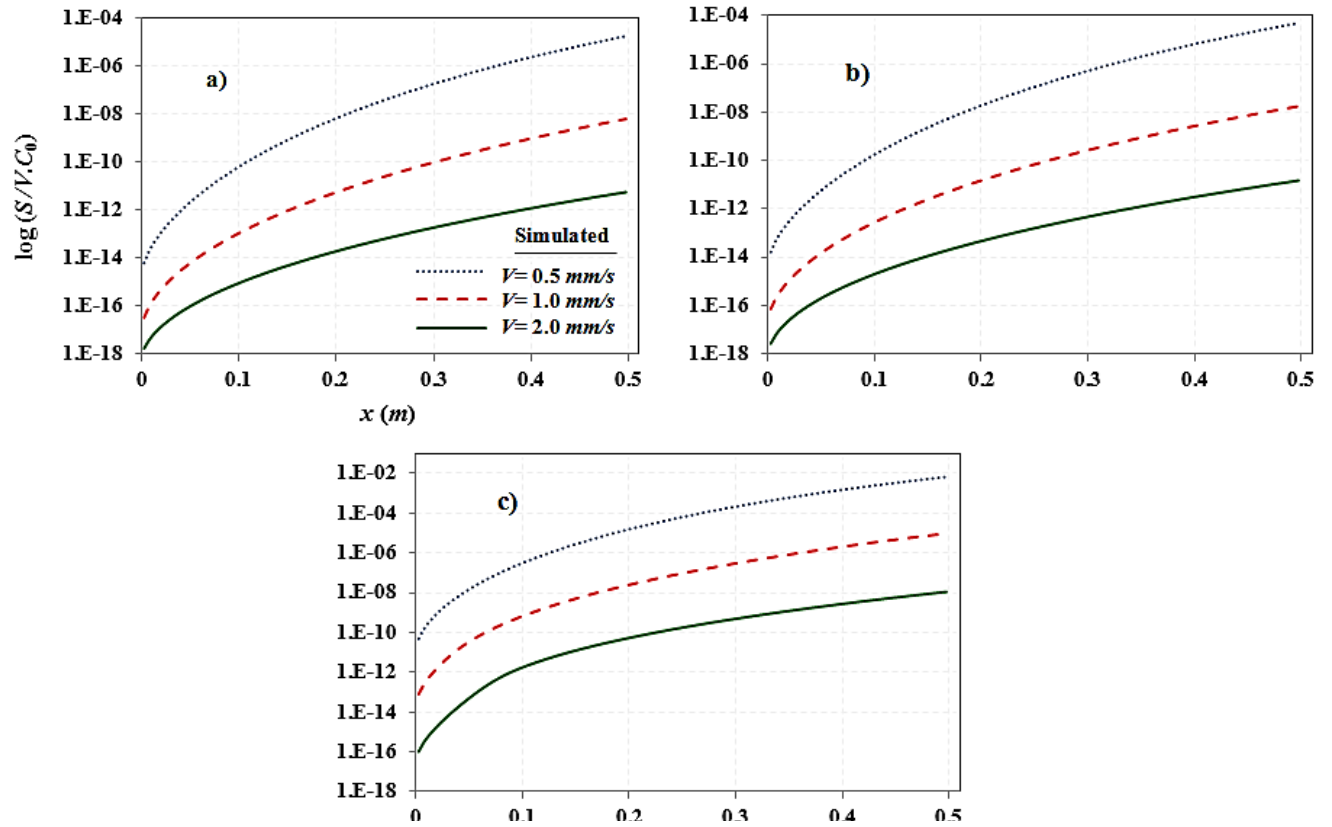
Figure (A2): Simulated normalized retained particle concentration profiles in different velocities (V) and C_0: a) $C_0 = 2$ g/l, b) 5 g/l, and c) 12 g/l. All profiles are calculated and/or measured at the end of the transport test.

Table (S1): Properties of porous medium, water and NZVI dispersion, and experimental conditions

Subject	Parameter	Value	Unit
Porous medium	Average diameter (d_{50})	0.83×10^{-3}	m
	Porosity (n)	0.37	-
	Longitudinal dispersivity (α_L)	5.7×10^{-3}	m
	Bulk density (ρ_b)	2670	Kg/m
	Hydraulic conductivity (K)	5.5×10^{-4}	m/s
	Permeability (k)	5.6×10^{-11}	m^2
Water (Karaj tap water)	Dynamic viscosity (μ_w)	0.89×10^{-3}	$Pa.s$
	Density (ρ_w)	997	Kg/m
	Ionic strength (I)	40	mM
	pH	≈ 7.0-7.3	-
NZVI dispersion	NZVI concentration(C)	2, 5, 8, 12	g/l
	Dynamic viscosity (μ_f)	0.89×10^{-3}	$Pa. s$
	Density of suspension (ρ_f)	(1.01, 1.03, 1.05, 1.08) $\times 10^3$	kg/m

Operating conditions	Temperature (T)	24 ($\pm 1\,^{\circ}$C)	$^{\circ}C$
	Pore water velocity(V)	$(0.5,\ 1,\ 2) \times 10^{-3}$	m/s

Table (A2): The R^2 and P-value (with $\alpha=0.05$) between the observed and simulated values of ΔP and C/C_0 for different experimental conditions.

Variable	C_0 (g/l)	$V= 0.5mm/s$		$V= 1.0mm/s$		$V= 2.0mm/s$	
		R^2	P-value	R^2	P-value	R^2	P-value
ΔP	2	0.970	0.505	0.967	0.377	0.993	0.724
	5	0.965	0.739	0.974	0.591	0.982	0.435
	8	1.000	0.010*	1.000	0.191	1.000	0.033*
	12	0.998	0.641	0.998	0.764	1.000	0.485
C/C_0	2	1.000	0.875	1.000	0.791	1.000	0.935
	5	0.999	0.746	1.000	0.773	1.000	0.822
	8	0.996	0.651	0.998	0.733	0.997	0.709
	12	0.988	0.520	0.746	0.016*	0.998	0.381

* Significance level of 95%.